# Contribution of energetic and heavy ions to the plasma pressure: Storm September 27 - October 3, 2002

E. A. Kronberg[1,2], L. M. Kistler[3], D. Welling[4], C. Mouikis[3], P. W. Daly[1], E. E. Grigorenko[5], B. Klecker[6], and I. Dandouras[7,8]

Author Manuscript

Key points:

1. The contribution of ions of different species to the total plasma pressure in the near-Earth magnetosphere is estimated.
2. The ability of the Space Weather Modeling Framework to reproduce the plasma pressure during a magnetic storm is tested.
3. The main source of oxygen ions is located at distances Earthward of XGSE$\simeq$-13.5 $R_E$ during the main phase.

[1]Max Planck Institute for Solar System

This is the author manuscript accepted for publication and has undergone full peer review but has not been through the copyediting, typesetting, pagination and proofreading process, which may lead to differences between this version and the Version of Record. Please cite this article as doi: 10.1002/2017JA024215



This article is protected by copyright. All rights reserved.

**Abstract.** Magnetospheric plasma sheet ions drift towards the Earth and populate the ring current. The ring current plasma pressure distorts the terrestrial internal magnetic field at the surface and this disturbance strongly affects the strength of a magnetic storm. The contribution of energetic ions (>40 keV) and of heavy ions to the total plasma pressure in the near-Earth plasma sheet is not always considered. In this study, we evaluate the con-

Research, Göttingen, Germany

[2]Ludwig Maximilian University of Munich, Munich, Germany

[3]University of New Hampshire, Durham, NH, USA

[4]University of Michigan, Ann Arbor, USA

[5]Space Research Institute, Russian Academy of Sciences, Moscow, Russia

[6]Max Planck Institute for extraterrestrial physics, Garching, Germany

[7]University of Toulouse, UPS-OMP, UMR 5277, Institut de Recherche en Astrophysique et Planátologie (IRAP), Toulouse, France

[8]CNRS, IRAP, Toulouse, France

Author Manuscript



This article is protected by copyright. All rights reserved.

tribution of low-energy and energetic ions of different species to the total plasma pressure for the storm observed by the Cluster mission from September 27 until October 3 in 2002. We show that the contribution of energetic ions (>40 keV) and of heavy ions to the total plasma pressure is ≃76–98.6% in the ring current and ≃14–59% in the magnetotail. The main source of oxygen ions, responsible for ≃56% of the plasma pressure of the ring current, is located at distances Earthward of XGSE≃-13.5 $R_E$ during the main phase of the storm. The contribution of the ring current particles agrees with the observed *Dst* index. We model the magnetic storm using the Space Weather Modeling Framework (SWMF). We assess the plasma pressure output in the ring current for two different ion outflow models in the SWMF through comparison with observations. Both models yield reasonable results. The model which produces the most heavy ions agrees best with the observations. However, the data suggests that there is still potential for refinement in the simulations.

Author Manuscript



This article is protected by copyright. All rights reserved.

## 1. Introduction

This study was initiated by the Geospace Environment Modeling (GEM) focus group on "the ionospheric source of magnetospheric plasma". The aim of this group is to quantify the importance of the ionospheric source in magnetospheric dynamics. Observations from different satellites and modeling results were compared. For this study, the magnetic storm which occured from September 27 until October 3, 2002 was chosen. This event is a prime opportunity for data-model comparison because of its strength and extensive data availability. During this event, the constellation of spacecraft such as Fast Auroral Snapshot Explorer (FAST), Polar and Cluster allows us to follow the ionospheric ion distributions from the polar region to the lobes, the plasma sheet and eventually to the ring current region. This gives us an opportunity to validate numerical models at different stages of the ionospheric ion circulation.

The circulation of the ionospheric ions in the magnetosphere is shown in Figure 1. The ions flow from the polar regions of the ionosphere including the auroral region, cusp region and the polar cap (polar wind). Polar wind and cusp ions flow into the lobe where they either get lost in the solar wind (through the distant tail) or convect into the plasma sheet and get trapped. It is shown by *Haaland et al.* [2015] that during a storm, the polar cap expands and the strength of the ion outflow increases by almost an order of magnitude. Ions from the auroral region enter the plasma sheet directly. The ions in the plasma sheet are accelerated by different mechanisms (for example by the non-adiabatic Speiser acceleration, which is shown in the figure by wavy line), they drift westward and towards the Earth and lead to the increase of the plasma pressure especially in the ring current



This article is protected by copyright. All rights reserved.

region (shown by the red arrow). A more detailed review on the circulation of heavy ions can be found in *Kronberg et al.* [2014].

There are a number of studies on the contribution of ions of different species and energies to the ring current. The contribution of the most representative ionospheric ion, oxygen, to the energy density during storms was estimated to vary from 25% to 47% [*Krimigis et al.*, 1985; *Hamilton et al.*, 1988; *Roeder et al.*, 1996; *Zhao et al.*, 2015]. *Greenspan and Hamilton* [2002] did a statistical study of the contributions of $O^+$ and $H^+$ over the energy range from 1.5 to 300 keV/e for 67 magnetic storms. They show that ions of ionospheric origin contribute ∼20%–∼150% of the ring current energy density of protons during the maximum of the magnetic storms. The contribution of helium is not more than 3% during quiet times [*Pulkkinen et al.*, 2001] and 5% during a magnetic storm [*Hamilton et al.*, 1988]. *Kronberg et al.* [2012] showed that the energy density of oxygen at energies >270 keV can be higher than the energy density of protons at distances between 6 and 10 $R_E$ during magnetic storms. For ions with ≃10 keV, the oxygen contribution is about 20%.

Previous studies still disagree on the partition of the most contributing energies during quiet and stormy times. For example, *Krimigis et al.* [1985] using AMPTE CCE observations found that the ring current is dominated by protons at energies ≃100–300 keV during both quiet and intense storm times. Other studies show that the contribution of energetic ions into the ring current is more significant during quiet times than during storm times [e. g. *Williams*, 1981; *Zhao et al.*, 2015; *Gkioulidou et al.*, 2016]. *Gkioulidou et al.* [2016] indicated that the high-energy (> 100 keV) proton component to the ring current pressure shows no correlation with the activity level (SYM-H index) and is domi-



This article is protected by copyright. All rights reserved.

nating during non-storm times. The low-energy (<80 keV) proton component is strongly governed by convective timescales and is very well correlated with the absolute value of the SYM-H index, controlling the pressure during storm times. Other studies report different dominant energy ranges, e.g. ≃210 keV during quiet times and ≃85 keV during storm times (observations from Explorer 45 by *Williams* [1981]) and >100 keV and <50 keV, respectively (recent comprehensive observations by Van Allen Probes by *Zhao et al.* [2015]).

The contribution of energetic protons (>40 keV) and of heavier ions (He, $O^+$) in the total plasma pressure is considered in some models, e. g., the Comprehensive Ring Current Model (CRCM, *Fok et al.* [2001]) and the ring current-atmosphere interactions model (RAM, *Jordanova et al.* [1997]). In most models of the terrestrial magnetosphere, however, the contribution is not considered. For example, the empiric models for ion plasma parameters by *Tsyganenko and Mukai* [2003] and *Borovsky et al.* [1998], which are commonly used for boundary conditions in models of the inner magnetosphere, are based on data of ions with energies less than 40 keV. Also, the empirical models of ion fluxes by *Denton et al.* [2015, 2016], which consider ions with ∼1 eV to ∼40 keV at geosynchronous orbit without resolving the species, can only be used to estimate the partial plasma pressure. This omission can be justified for ions at energies higher than >270 keV. During an average substorm and at radial distances R>6 $R_E$, the corresponding partial pressure is <2% [*Kronberg et al.*, 2015]. However, ions at energies between 40 keV and 270 keV must be considered in models of the ring current. These additional particle populations can increase the ring current plasma pressure which distorts the terrestrial magnetic field.



This article is protected by copyright. All rights reserved.

These energies are considered, for example, in the empirical model for electron plasma sheet densities and temperatures by *Dubyagin et al.* [2016].

In this study, we use observations by the Cluster satellites. The advantage of this mission is availability of ion composition measurements, a broad energy range (from ≃40 eV to 1 MeV ) and the orbital coverage of both the ring current and the magnetotail region. For the first time, we estimate the contribution of different ion species at two energy ranges to the plasma pressure both in the magnetotail and the ring current during the development of a magnetic storm. The comparison of two different regions may give us a hint on which mechanisms are effective in populating the ring current and on the location of ion sources. We estimate the contribution of the derived plasma pressure to the *Dst* index and compare it with the observed one. For the first time, we compare the observed plasma pressure in the ring current for this magnetic storm event with simulations of the Space Weather Modeling Framework (SWMF) [*Tóth et al.*, 2005, 2012], which take into account ionospheric ion outflows from two different models. We assess our current capability to reproduce the ionosphere-magnetosphere coupling.

## 2. Instrumentation and data

The Cluster spacecraft are flying in a tetrahedron-like formation in polar orbit around the Earth since the end of the year 2000. More information about the Cluster mission and its instrumentation is given in *Escoubet et al.* [1997].

The low-energy component of the pressure, $P_{\mathrm{CIS}}$, for protons, helium and oxygen at ∼40 eV/q–40 keV/q is derived from observations by the Cluster Ion Spectrometry (CIS) using the time-of-flight ion Composition Distribution Function (CODIF) sensor [*Rème et al.*, 2001]. The inflight calibration for protons and heavy ions is continuously updated



Author Manuscript

This article is protected by copyright. All rights reserved.

for CIS [*Kistler et al.*, 2013]. Background contamination in the ring current region is corrected for using a procedure from *Mouikis et al.* [2014].

The contribution of energetic ions at energies >40 keV is calculated from the observations by the Research with Adaptive Particle Imaging Detector (RAPID) [see *Wilken et al.*, 2001] and its Imaging Ion Mass Spectrometer (IIMS). The energy ranges are 27.7 keV – 4 MeV for protons, 138 keV –3.8 MeV for helium and 274 – 4 MeV for the CNO group [*Daly and Kronberg*, 2010]. No information about the charge state of the ion species is possible. For simplicity, we will write $H^+$, $He^+$ and $O^+$ for hydrogen, helium and the CNO group, respectively, in the case of RAPID data. The energetic particle partial pressure for the RAPID measurements is calculated using the formula

$$P_{\mathrm{RAPID}}[\mathrm{nPa}] = 4\pi\frac{2}{3}0.518\cdot 10^{-8}\sqrt{m[\mathrm{amu}]}\sqrt{E[\mathrm{keV}]}J[\mathrm{cm}^{-2}\mathrm{sr}^{-1}\mathrm{s}^{-1}], \quad (1)$$

where $m$ is the ion mass in atomic mass units (amu), $J$ is the integral intensity and $E$ is the effective energy calculated as the geometric mean. The validity of the latter assumption is established in *Kronberg and Daly* [2013].

The first proton RAPID energy channel at 27.7 –64.4 keV overlaps with the last CIS energy channels. In order to obtain a continuous spectrum we truncate the first RAPID channel. The CIS and the RAPID instruments are well cross-calibrated for protons, see [*Kronberg et al.*, 2010].

Heavy ions cannot be cross-calibrated because of a large gap between the energy channels (CIS/CODIF measures ions up to $\simeq$40 keV for both $He^+$ and $O^+$, whereas RAPID/IIMS starts to detect $He^+$ ions at 138 keV and $O^+$ ions at 274 keV). The calibration factors (efficiencies) for RAPID for the heavy ions were derived prior to its launch. The relative efficiency of the heavy ions with respect to protons is assumed to be constant



This article is protected by copyright. All rights reserved.

during the mission. As the magnetic storm studied here is observed at the beginning of the mission and the proton measurements by CIS and RAPID show a good agreement, the data on heavy ions should also be reliable.

For the $He^+$ and $O^+$ observations, the data gap between the CIS/CODIF and the RAPID/IIMS measurements is fitted using a power law, because this gap is in the descending part of the energy spectrum, see [e. g. *Kistler et al.*, 1990] for the plasma sheet and [*Kistler et al.*, 1994; *Keika et al.*, 2016] for the ring current. The power law fit is an approximation that in most cases may lead to an underestimation of the partial pressure. Because we do only a rough estimation of the relative contribution of different species and because we are not interested in fine structure of the ion spectra to the ion pressure, we consider this approximation to be feasible. We refer to the part of the pressure derived from the power law fit together with the pressure derived from the RAPID observations as the energetic pressure or the RAPID pressure.

## 3. Model

To model this storm, the Space Weather Modeling Framework (SWMF) [*Tóth et al.*, 2005, 2012] is used to combine the Block Adaptive Tree Solar wind Roe-type Upwind Scheme (BATS-R-US) [*Powell et al.*, 1999; *De Zeeuw et al.*, 2000; *Welling and Ridley*, 2010] multi-species magnetohydrodynamic (MHD) model, an ionospheric electrodynamics model [*Ridley et al.*, 2001], and an ionospheric outflow model. Two outflow models are used in this study: the Polar Wind Outflow Model (PWOM) and the Generalized Polar Wind (GPW) model. The SWMF uses observed upstream solar wind and interplanetary magnetic field (IMF) values to drive the MHD model. The density and the radial velocity of $H^+$ and $O^+$ at the MHD inner boundary (a sphere of 2.5 $R_E$) are taken from the results



Author Manuscript

This article is protected by copyright. All rights reserved.

of one of the outflow models. The MHD density and pressure moments are interpolated in time and space to the position of the Cluster 1 spacecraft for data to model comparisons. The model setup and configuration follows that of *Welling et al.* [2016].

The first ionospheric outflow model used in this study is the Polar Wind Outflow Model (PWOM) [*Glocer et al.*, 2009a; *Welling et al.*, 2011; *Glocer et al.*, 2012]. This model solves the gyrotropic transport equations for ions and electrons along many independent magnetic flux tubes. As input, PWOM receives the field-aligned currents (FACs) from other SWMF codes. The topside electron velocity is set assuming charge neutrality and current conservation. Changes in the current flow compress or rarefy the electron fluid, altering the ambipolar field and driving outflow fluxes [*Gombosi and Nagy*, 1989; *Welling et al.*, 2015].

The second model is the Generalized Polar Wind (GPW) model [*Schunk and Sojka*, 1989; *Sojka and Schunk*, 1997; *Barakat and Schunk*, 2006]. Below an altitude of 1200 km, GPW solves the same fluid equations as PWOM. Above this altitude, however, a fully kinetic Particle-In-Cell (PIC) approach is taken. This allows GPW to take into account many acceleration mechanisms, including the effects of wave-particle acceleration and collisions [*Barakat and Schunk*, 2001]. Unlike PWOM, GPW is run independently of the SWMF and is later used as input for the MHD code. It utilizes the observed geomagnetic indices and empirical electric fields as input (for details, see *Barakat et al.* [2015]). Because of the additional acceleration mechanisms included in GPW, it tends to produce faster and denser outflows compared to the PWOM model, as well as more polar cap and day side outflow [*Welling et al.*, 2016]. These source populations advect deeper



This article is protected by copyright. All rights reserved.

down the tail in the magnetosphere, where they are more effectively heated in the plasma sheet compared to PWOM populations [*Yu and Ridley*, 2013; *Welling et al.*, 2016].

PWOM and BATS-R-US are brought to a pseudo-steady state using the solar wind conditions present at the start of the simulation time line. Because GPW only uses geomagnetic indices as input, it was started earlier to build realistic conditions at the time of the SWMF simulation start.

We have decided that the simulation start is on October 1st, 00:00 UT for a few reasons. We typically start runs a few hours before storm sudden onsets. This poses a challenge for starting the simulation of our event: we can either start with the arrival of the storm sudden commencement at ≃08:00 UT on September 30, or wait until after the two pressure pulses that mark the beginning of the storm on the same day until ≃22:00 UT (see Figure 2). However, the Solar Wind Electron Proton Alpha Monitor (SWEPAM) data is not available before the two solar wind density peaks. The simulations are also costly and adding an additional day to the current simulation would greatly extend the time to perform the simulation. These factors together drove our decision to start the simulation on October 1st.

We do not include an inner magnetospheric model in the simulations. On the dayside, the inclusion of an inner magnetospheric model, such as the Rice Convection Model (RCM) would push the results to warmer temperatures and pressures. However, the effect of magnetic shielding would limit this effect: as inner magnetosphere pressure builds, the field stretches via force balance, and closed drift paths are relegated to low L-shells. The hotter plasma is therefore more likely to drift out of the inner magnetosphere before it reaches the dayside.



This article is protected by copyright. All rights reserved.

## 4. Observations

The measurement of the change of the horizontal component of the terrestrial magnetic field, represented by the SYM/H index, is shown in Figure 2 in the bottom panel. This is an intensive (SYM/H $\simeq$ -150 nT) and long lasting magnetic storm associated with powerful solar wind dynamic pressure pulses (panel c) and negative excursion of the IMF $B_z$ magnetic field component associated with a coronal mass ejection (panel a). This event is also discussed in *Haaland et al.* [2015] and *Kistler et al.* [2010].

The trajectory of Cluster 1 during this event is shown in Figure 3.

We calculate the plasma pressure for the selected time intervals before the magnetic storm, during its main phase and the recovery phase. We choose time periods that include spacecraft crossings of the neutral plane. The blue and green vertical bars in Figure 2 show time intervals for which pressure calculations were performed and shown in Figures 4 and 5. The locations of the spacecraft during the time intervals for which the plasma pressure is calculated are highlighted by blue and green bars in Figure 3. In Table 1, we present the percentage, of the particular partial pressure (different ion species and energy) to the total plasma pressure including all species and energies close to the neutral plane (20–40 minutes of observations around the crossing). To see the development of every particular partial pressure, we compare the pressures during the storm with those before the magnetic storm onset. The corresponding ratios are listed in Table 2. We list the relative contribution of low-energy to energetic pressures in Table 3.

Figure 4 (left) shows the plasma pressure and the magnetic field during the pre-storm time (September 28), marked by the first blue bar in Figure 2 when Cluster 1 was in the magnetotail plasma sheet at XGSE$\sim$-17 $R_E$. The data collected during the recovery phase



This article is protected by copyright. All rights reserved.

shown in the right panel of Figure 4 is discussed later. The partial pressure calculations are done for different species and at different energies (low-energy and energetic), see the left column top panel of Figure 4. The panel below shows the magnetic field components: the thick line represents $B_x$, the bottom line represents $B_y$ and the top line represents $B_z$ in GSE. This is a very quiet central plasma sheet. According to CIS $H^+$ observations close to the neutral plane, the partial pressure of the low-energy population is $P_{H+CIS}$= 86% between 06:45 and 07:15 UT, see Table 1. We note that in the near-Earth magnetotail, there are almost no energetic particles ($\leq$ 1.5%) and about 8.9% low-energy oxygen ions, which is already a significant fraction, see Table 1.

The second bar in Figure 2 (green-colored) represents the pre-storm time period (on September 29) when Cluster 1 was in the ring current region. The satellite crossed the neutral plane at the dayside during this time. The partial pressure calculations for this time period are shown in the left column of Figure 5. The meaning of the line colors is the same as described above. The pressure calculations close to the neutral plane are done for the time period from 12:40 to 13:00 UT, see Tables 1, 2 and 3. The pre-storm ring current is mainly ($\simeq$82.9%) populated by energetic protons with energies $>$ 40 keV. The difference in the low-energy and energetic pressures (according to CIS and RAPID measurements, respectively) becomes more prominent towards the neutral plane. Here our estimations of the contribution of helium during quiet time are higher than those of *Pulkkinen et al.* [2001]. In the study of *Pulkkinen et al.* [2001], the highest energy considered in the calculations is 200 keV, however. If we limit our energy range by this value, we get the same result.



This article is protected by copyright. All rights reserved.

The third bar in Figure 2 (green-colored) represents the main phase of the magnetic storm (October 1). The passage of Cluster 1 is almost identical (just a bit shorter) to the one at the pre-storm time shown in Figure 3. However, the plasma pressure is significantly different during this time period, see the right-hand column Figure 5 . The total pressure close to the neutral plane increases $\simeq$2 times at $L \simeq$5 between 22:10 and 22:30 UT. The relative amount of protons measured by CIS in the ring current is 1.4% during pre-storm time and to 23.8% during the main phase.

The low-energy proton pressure increases $\simeq$34 times during the storm phase. Energetic protons dominate the ring current before the magnetic storm, see Table 2. During the storm, low-energy protons dominate. This may be related to the activation of a plasmaspheric source, enhanced transport from the polar cap, which brings ions closer to the Earth [e. g., *Li et al.*, 2013], or transport from the solar wind during the magnetic storm. We cannot distinguish between these sources of protons. At the same time, the energetic proton pressure decreases by a factor of $\simeq$0.27 during the magnetic storm, see Table 2. This can in part be explained by the short/long lifetimes of the low-energy/energetic protons due to charge exchange. Therefore, energetic protons stay in the ring current for a long time during quiet period whereas low-energy protons get lost.

The most dramatic increase during the storm, however, is associated with oxygen ions. $O^+$ ions with energies $<$ 40 keV ($>$40 keV) contribute $\simeq$26% ($\simeq$29.5%) of the total pressure. In total, ionospheric ions ($O^+$) contribute about 55.5% (and with helium this is about $\simeq$64.9%) of the total pressure. This is somewhat higher than the previous estimations of the ion contributions for oxygen (up to 47%) and helium (5%) discussed in Section 1. This can again be explained by the wider energy range considered in our study and by



This article is protected by copyright. All rights reserved.

the importance of the contribution of energetic ions. The numbers imply that simulations of the geospace environment will be wrong if ionospheric (oxygen) ions are neglected.

The results of SWMF simulations coupled with PWOM are represented by the solid black line in Figure 5. It agrees with the partial pressure, $P_{CIS}$, of protons with $< 40$ keV. The model underestimates the plasma pressure by a factor of $\leq$3.5. This outflow model delivers too small ion densities which are not reliable for the use as boundary conditions. This is one of the reasons that can explain the observed discrepancy in the plasma pressure. The simulations of the model coupled with GPW are represented by the solid red line in Figure 5. This model shows good agreement with the partial pressure including CIS $H^+$+RAPID $H^+$+CIS $O^+$ components. The model with the GWP input reproduces the plasma pressure within a factor of $\simeq$2. This model does not include helium ions. It, however, overestimates the pressure in the regions at higher-latitudes (before 21:30 UT and after 23:20 UT). The overestimation at higher latitudes is possibly caused by an overproduction of oxygen in the GWP model. The discrepancy in the region close to the neutral plane is associated with the omission of the cusp source and non-adiabatic acceleration mechanisms in the plasma sheet.

The fourth bar in Figure 2 (blue-colored) represents the recovery phase of the storm (October 2). The partial plasma pressure and the magnetic field observations in the magnetotail for this time period are shown in Figure 4 (right panels). The satellites were located at XGSE$\simeq$-13.5 $R_E$, see Figure 3. The satellite was approaching the plasma sheet center but did not cross it. Therefore, we consider only the closest approach to the current sheet neutral plane (from 13:00 to 13:40 UT) in the pressure calculations. During this time period, the sudden increase of the ion intensities is associated with an energetic



Author Manuscript

This article is protected by copyright. All rights reserved.

particle injection accompanied by magnetic field dipolarizations that are reflected in the growth of the $B_z$ component at ≃12:48, 13:10 and 13:29 UT. The preferential increase of the energetic ion flux during dipolarizations was discussed extensively by *Moebius et al.* [1987] and *Kistler et al.* [1990]. *Kistler et al.* [1992] show that the pressure (energy density) is carried by the higher energy ions during injections. They also suggest that the increase of the plasma pressure results from the conservation of pressure equilibrium and does not necessarily indicate that local changes in the field are accelerating the particles. During the recovery phase, energetic oxygen and helium ions dominate over those at low energies (the ratios of $P_{CIS}/P_{RAPID}$ are 0.82 and 0.44, respectively, see Table 3) in agreement with *Kistler et al.* [1992]. During this phase we observe an efficient with respect to the pre-storm magnetotail acceleration of heavy ions (oxygen and helium) as well as of protons. The magnetic field in Figure 4 (right bottom panel) shows turbulent fluctuations which are not seen in the quiet magnetic field observed before the magnetic storm (left bottom panel). The energetic particle pressure changes by a factor of ≃28 and 357 compared to the low energy part, which basically stays the same at least for the protons and oxygen, see Table 2. The strongest increase of the energetic ion intensities is associated with dipolarization events with signatures of magnetic field turbulence (at ≃12:48–12:58 and ≃13:29–13:40 UT). During these events, the sum of the magnetic and plasma pressures is enhanced (not shown). An effective acceleration of ions by turbulence during magnetic field dipolarizations can lead to strong ion intensity increases [*Grigorenko et al.*, 2017]. If we divide the ratios of energetic oxygen and helium from Table 2 with those of the protons we obtain ≃12 and ≃2.3. This implies that the acceleration mechanism is mass/charge dependent. In contrast to *Kistler et al.* [1992], we suggest that the ion acceleration plays



Author Manuscript

This article is protected by copyright. All rights reserved.

an important role in the increase of the ion pressure during this event. Therefore, it is important to include the non-adiabatic ion acceleration in the plasma sheet in models or, alternatively, include energies >40 keV in models of boundary conditions in the near-Earth plasma sheet.

The total ion pressure in the tail close to the neutral plane has grown by a factor of $\simeq$1.6 between the two time periods. However, the low-energy proton pressure is approximately the same, see Table 2. Consideration of only low-energy protons (without energetic ions and other species) will underestimate the pressure by $\simeq$49% during the recovery phase.

The modeling (black line along the time-axis) fails to describe the magnetotail observations because the SWMF misses the plasma sheet encounter and virtual Cluster is still in the lobe. It is known that modern magnetospheric models still have difficulties to predict the position of the magnetotail during disturbed times. The predicted plasma pressures are very low and correspond with the pressures in the lobe region.

Low-energy and energetic $O^+$ make approximately equal contributions to the pressure in the ring current region, independent of the geomagnetic disturbance level (3.1% and 4.6% during quiet time; 26% and 29.5% during disturbed time), see Table 1. The same is not true in the tail region, where during storm times the contribution of energetic $O^+$ to the total pressure increases by a factor of $\simeq$223. The discrepancy in the ratios implies that ion sources Earthward of XGSE$\simeq$-13.5 $R_E$ are important for the ring current dynamics.

We assess the effectiveness of the ion acceleration by comparing the ratios of the low-energy to energetic pressures before and during the magnetic storm in Table 2. We calculate the following ratio for $H^+$, $He^+$ and $O^+$:

$$(P_{\text{RAPID during}}/P_{\text{RAPID before}})/(P_{\text{CIS during}}/P_{\text{CIS before}}).$$



This article is protected by copyright. All rights reserved.

Author Manuscript

The ratios are ≃30, ≃360 and ≃30 for the tail part and ≃0.08, ≃0.12 and ≃0.84 for the ring current. This shows that the acceleration processes strongly dominate the energy distribution of the magnetotail plasma population. In the ring current, we observe a decrease of the proton plasma pressure between times before and during the magnetic storm (see Figure 5). This means that energetic protons accelerated in the magnetotail were removed from the ring current during the magnetic storm, for example due to a change of closed drift paths to lower L-shells. Here we assume that the ratio of low-energy and energetic pressures in the tail during the recovery phase is at least as high as during the main phase, because the low-energy population does not react strongly to the *Dst* index [*Kronberg et al.*, 2012; *Maggiolo and Kistler*, 2014]. This leads to a decrease of the ratio. The anticorrelation of the energetic particle content with the main magnetic storm phase was also shown by *Gkioulidou et al.* [2016]. The plasma pressure of low-energy ions in the magnetotail is approximately the same before the magnetic storm and during the recovery phase. Therefore, the magnetotail can not be a significant source of low-energy particles. This again implies that there is an effective low-energy ion source Earthward of XGSE≃-13.5 $R_E$. The relation between sources and sinks deserves more extensive attention in future studies.

## 5. Discussion

Particle inflow, reflected by an increase of the plasma pressure, leads to increase of magnetic field distortion. We estimate if the depression of the magnetic field, as reflected in the SYM/H index, $\Delta B \simeq$ -140 nT (values of the Dst index on September 29 at ≃13:00 (36 nT) and October 1 at ≃22:15 (-104 nT) are used), corresponds to a change of the plasma pressure. For this we use the Dessler-Parker-Scopke expression [*Dessler and Parker*, 1959;



This article is protected by copyright. All rights reserved.

*Sckopke*, 1966]:

$$\Delta B = -\frac{2U_R B_E}{3U_M}, \tag{2}$$

where $U_R$ is the total energy of all ring current particles, $U_M$ is the total energy of the main Earth's dipole field above its surface and $B_E$ is the magnetic field on the Earth's surface at the equator. The total energy of all ring current particles can be calculated as follows:

$$U_R = 3/2\Delta PV, \tag{3}$$

using $PV = nkT$, where $n$ is the plasma density, $k$ is the Boltzmann constant, $T$ is the plasma temperature, $P$ is the plasma pressure and $V$ is the volume of the ring current. The magnetic energy is estimated as $U_M = 4\pi B_E^2 R_{\rm E}^3/(3\mu_0)$, where $B_E = -\mu_0 M/(4\pi R_{\rm E}^3) = 3.11 \cdot 10^{-5}$T, $\rm R_E$ is the radius of the Earth, $\mu_0$ is the magnetic permeability and $M = 8 \cdot 10^{22}\rm A \cdot m^2$ is the magnetic moment of the Earth. We calculate the volume of the ring current using equation (2.10) from *Lyons and Williams* [1984] and assuming that the ring current is located between $L$-shells 2.5 and 7 [*Vallat et al.*, 2005; *Grimald et al.*, 2012; *Liemohn et al.*, 2015]. If we use only low-energy pressure from protons $\rm P_{CIS\ H+}$ (blue dashed lines) and take $\Delta P \simeq$1.5 nPa, we get the magnetic field depression of about -9 nT ($\simeq$3 times less than predicted, see discussion later). Using the total plasma pressure $\rm P_{CIS+RAPID}$ (black dashed lines) and taking $\Delta P \simeq$4 nPa, we get $\simeq$-24 nT. The pressure of electrons at this region is small (max. 0.2 nPa which would produce an additional $\simeq$1.2 nT estimated from Equation 3). Data from the PEACE instrument [*Johnstone et al.*, 1997] are used for this estimation. Therefore, the contribution of the ring current particles (symmetric current) to the SYM/H index is -24 nT+1.2 nT = $\simeq$-22.8 nT.



This article is protected by copyright. All rights reserved.

Other factors may also influence the SYM/H index. These are the magnetopause currents, the near-Earth cross-tail current, the partial ring current and the induction currents [*Kamide and Chian*, 2007].

The change of the SYM/H index due to the magnetopause current can be estimated using the expression $a\sqrt{p_{sw}^{dyn}}$, where $\sqrt{p_{sw}^{dyn}}$ is the solar wind dynamic pressure and $a$ is a coefficient. We take $a$ =3.63/(nPa)$^{1/2}$, because this storm has occurred during a southward IMF [*O'Brien and McPherron*, 2000]. The solar wind dynamic pressure can be estimated from Figure 2; we use $p_{sw}^{dyn}$ =5 nPa. Therefore, the magnetopause current will produce a magnetic field compression of ≃8 nT. The total contribution of the partial ring current and the near-Earth cross-tail currents to the magnetic field depression is (-16+0.29· SYM/H)/1.3 [*Kamide and Chian*, 2007]. Therefore, it is ≃ -37 nT using the observed SYM/H= -110 nT in Figure 2.

If we include the induction currents then the total magnetic depression has to be multiplied by a factor 1.3 [*Kamide and Chian*, 2007]. Therefore, utilizing our estimations above, we add the contributions of the ring current particles, the magnetopause current, the partial current and near-Earth cross-tail current and multipy the result by a factor 1.3: 1.3×(-22.8 nT+8 nT-37 nT). The result is ≃-68 nT, which is less than observed. It is possible that the contribution of the magnetotail current is about 50% according to *Alexeev et al.* [1996] and *Dremukhina et al.* [1999]. However, our estimations agree well with the prediction by *Kamide and Chian* [2007] that the symmetric ring current produces a magnetic field depression of (-4.6+0.27· SYM/H)/1.3, which is -26 nT. The consideration of ion components ($O^+$ and $He^+$) in addition to protons and an extended energy range (including >40 keV) significantly improves the comparison.



This article is protected by copyright. All rights reserved.

We assumed that all ions detected in the $O^+$ channels of the CODIF and RAPID instruments are indeed $O^+$. However, given the finite mass resolution of these instruments, $N^+$ ions could also be part of this population. $N^+$ ions have been observed to take substantial proportions in the ring current population during strong geomagnetic storms [*Hamilton et al.*, 1988].

## 6. Conclusions

In this study, we compared the contribution of different ion species and energies to the plasma pressure in the ring current and the magnetotail before and during the magnetic storm from September 27 until October 3 in 2002 for the first time. The results show that before the storm has initiated (September 28), the contribution of energetic ions to the total pressure is negligible in the tail plasma sheet, less than $\simeq$2%. The contribution of low-energy heavy ions is about 12%. However, as the storm evolves towards the main and recovery phase, the contribution of energetic and heavy ions to the pressure of the plasma sheet becomes significant, $\simeq$49%, and cannot be neglected. They must be included in models for ion plasma parameters of the plasma sheet. The contribution of energetic ions to the pressure of the ring current is significant before ($\simeq$95%) and during ($\simeq$49%) the magnetic storm. We demonstrate that heavy ions play a dominant role in the plasma pressure, contributing about 65% during the main phase. The main source of oxygen ions, responsible for $\simeq$56% of the plasma pressure of the ring current, is located at distances Earthward of XGSE$\simeq$-13.5 $R_E$ during the main phase of the storm.

Our estimations of the contribution of the ring current particles in the *Dst* index agree well with observations and demonstrate the importance of taking the ion composition into account and using an extended energy range.



This article is protected by copyright. All rights reserved.

Our study is in agreement with the work of *Williams* [1981]; *Zhao et al.* [2015]; *Gkioulidou et al.* [2016] which shows that ions at different energy ranges exhibit different dynamics during quiet geomagnetic times and magnetic storms. Low-energy ions with <40 keV play a negligible role in the ring current pressure during the geomagnetically quiet phase. We found that ion pressures below and above 40 keV contribute approximately equally to the total pressure during the magnetic storm. This is in agreement with studies by *Zhao et al.* [2015] and *Gkioulidou et al.* [2016]. We show that ions accelerated in the magnetotail do not contribute significantly to the ring current at the dayside during the main phase. In future works it is important to compare the contributions at different locations and during different phases of the magnetic storm, as it changes significantly during the storm's course (private communication with K. Keika).

It is necessary to consider heavy ions, especially ionospheric oxygen, in simulations of the terrestrial magnetosphere during disturbed times. In particular, empirical models for the plasma parameters used as input for inner magnetospheric models should be derived using observations of heavy ions and not their proxies. The models should also include the energetic part of the ion distribution in the calculations and, ideally, non-adiabatic acceleration mechanisms. The reproduction of the *Dst* index can be successful during the main phase of the magnetic storm, see [e. g. *Glocer et al.*, 2009b], as many energetic particles are lost, likely because closed drift path shrinks. However, during the recovery phase these particles must be considered, because they likely fill the ring current with energetic particles.

In this study we test the ability of the SWMF to reproduce the ion plasma pressure in the magnetosphere during this magnetic storm for the first time. As our and previous



This article is protected by copyright. All rights reserved.

studies show the importance of ionospheric ions, we used two models of ion outflow in the SWMF simulations. The results show that the model with the GWP input reproduces the plasma pressure within a factor of $\simeq$2 and it underestimates the plasma pressure within a factor of $\simeq$3.5 with the PWOM input. Overall, the GWP shows better results due to the inclusion of different acceleration processes. Because the magnetic field model fails to reproduce the tail dynamics, pressure estimations in the magnetotail were not relevant. This study shows that the SWMF reasonably reproduces the plasma pressure in the ring current. However, the modeling of the magnetosphere-ionosphere coupling can be improved especially in the magnetotail region. Additionally, the modeling results may somewhat underestimate the pressure because not all sources of ions, as e.g. the cusp, are taken into account.

**Acknowledgments.** We acknowledge the "Deutsches Zentrum für Luft und Raumfahrt (DLR)" for supporting the RAPID instrument at MPS under grant 50 OC 1602. E.E. Grigorenko thanks the Russian Scientific Foundation (project Nr. 14-12-00824) for the financial support. I. Dandouras thanks CNES for its support of the CIS instrument at IRAP. This work was initiated in the focus group at the GEM meeting on the "Ionospheric Source of Magnetospheric Plasma" led by R. Chappell, B. Schunk and D. Welling. The authors are grateful for the use of the OMNI data base for providing the AE, Dst and solar wind parameters. The Cluster data can be found in the CSA Archive: http://www.cosmos.esa.int/web/csa/.

## References

Alexeev, I. I., E. S. Belenkaya, V. V. Kalegaev, Y. I. Feldstein, and A. Grafe (1996),



This article is protected by copyright. All rights reserved.

Author Manuscript

Magnetic storms and magnetotail currents, *J. Geophys. Res.*, *101*, 7737–7748, doi:10.1029/95JA03509.

Barakat, A. R., and R. W. Schunk (2001), Effects of wave-particle interactions on the dynamic behavior of the generalized polar wind, *Journal of Atmospheric and Solar-Terrestrial Physics*, *63*, 75–83, doi:10.1016/S1364-6826(00)00106-1.

Barakat, A. R., and R. W. Schunk (2006), A three-dimensional model of the generalized polar wind, *J. Geophys. Res.*, *111*, A12314, doi:10.1029/2006JA011662.

Barakat, A. R., J. V. Eccles, and R. W. Schunk (2015), Effects of geographic-geomagnetic pole offset on ionospheric outflow: Can the ionosphere wag the magnetospheric tail?, *Geophys. Res. Lett.*, *42*(20), 8288–8293, doi:10.1002/2015GL065736.

Borovsky, J. E., M. F. Thomsen, and R. C. Elphic (1998), The driving of the plasma sheet by the solar wind, *J. Geophys. Res.*, *103*, 17,617–17,640, doi:10.1029/97JA02986.

Daly, P. W., and E. A. Kronberg (2010), RAPID Products at the Cluster Active Archive, in *The Cluster Active Archive, Studying the Earth's Space Plasma Environment*, edited by Laakso, H., Taylor, M., & Escoubet, C. P., pp. 145–158, doi:10.1007/978-90-481-3499-1_9.

De Zeeuw, D., T. Gombosi, C. Groth, K. Powell, and Q. Stout (2000), An adaptive MHD method for global space weather simulations, *IEEE Transactions on Plasma Science*, *28*(6), 1956–1965, doi:10.1109/27.902224.

Denton, M. H., M. F. Thomsen, V. K. Jordanova, M. G. Henderson, J. E. Borovsky, J. S. Denton, D. Pitchford, and D. P. Hartley (2015), An empirical model of electron and ion fluxes derived from observations at geosynchronous orbit, *Space Weather*, *13*, 233–249, doi:10.1002/2015SW001168.



Author Manuscript

This article is protected by copyright. All rights reserved.

Denton, M. H., M. G. Henderson, V. K. Jordanova, M. F. Thomsen, J. E. Borovsky, J. Woodroffe, D. P. Hartley, and D. Pitchford (2016), An improved empirical model of electron and ion fluxes at geosynchronous orbit based on upstream solar wind conditions, *Space Weather*, *14*, 511–523, doi:10.1002/2016SW001409.

Dessler, A. J., and E. N. Parker (1959), Hydromagnetic theory of geomagnetic storms, *J. Geophys. Res.,* , *64*, 2239–2252, doi:10.1029/JZ064i012p02239.

Dremukhina, L. A., Y. I. Feldstein, I. I. Alexeev, V. V. Kalegaev, and M. E. Greenspan (1999), Structure of the magnetospheric magnetic field during magnetic storms, *J. Geophys. Res.*, *104*, 28,351–28,360, doi:10.1029/1999JA900261.

Dubyagin, S., N. Y. Ganushkina, I. Sillanpää, and A. Runov (2016), Solar wind-driven variations of electron plasma sheet densities and temperatures beyond geostationary orbit during storm times, *J. Geophys. Res.*, *121*, 8343–8360, doi:10.1002/2016JA022947.

Escoubet, C. P., R. Schmidt, and M. L. Goldstein (1997), Cluster - Science and Mission Overview, *Space Sci. Rev.*, *79*, 11–32.

Fok, M.-C., R. A. Wolf, R. W. Spiro, and T. E. Moore (2001), Comprehensive computational model of earth's ring current, *J. Geophys. Res.*, *106*(A5), 8417–8424, doi:10.1029/2000JA000235.

Gkioulidou, M., A. Y. Ukhorskiy, D. G. Mitchell, and L. J. Lanzerotti (2016), Storm time dynamics of ring current protons: Implications for the long-term energy budget in the inner magnetosphere, *Geophys. Res. Lett.*, *43*, 4736–4744, doi:10.1002/2016GL068013.

Glocer, A., G. Tóth, T. Gombosi, and D. Welling (2009a), Modeling ionospheric outflows and their impact on the magnetosphere, initial results, *J. Geophys. Res.*, *114*, A05216, doi:10.1029/2009JA014053.



Author Manuscript

This article is protected by copyright. All rights reserved.

Glocer, A., G. Tóth, Y. Ma, T. Gombosi, J.-C. Zhang, and L. M. Kistler (2009b), Multi-fluid Block-Adaptive-Tree Solar wind Roe-type Upwind Scheme: Magnetospheric composition and dynamics during geomagnetic storms – Initial results, *J. Geophys. Res.*, *114*, A12203, doi:10.1029/2009JA014418.

Glocer, A., N. Kitamura, G. Toth, and T. Gombosi (2012), Modeling solar zenith angle effects on the polar wind, *J. Geophys. Res.*, *117*(A4), A04,318, doi:10.1029/2011JA017136.

Gombosi, T. I., and A. F. Nagy (1989), Time-dependent modeling of field-aligned current-generated ion transients in the polar wind, *J. Geophys. Res.*, *94*(A1), 359, doi:10.1029/JA094iA01p00359.

Greenspan, M. E., and D. C. Hamilton (2002), Relative contributions of $H^+$ and $O^+$ to the ring current energy near magnetic storm maximum, *J. Geophys. Res.*, *107*, 1043, doi:10.1029/2001JA000155.

Grigorenko, E. E., E. A. Kronberg, and P. W. Daly (2017), Heating and acceleration of charged particles during magnetic field dipolarizations, *Cosmic Research*, *55*, 57–66, doi:10.1134/S0010952517010063.

Grimald, S., I. Dandouras, P. Robert, and E. Lucek (2012), Study of the applicability of the curlometer technique with the four Cluster spacecraft in regions close to Earth, *Ann. Geophys.*, *30*, 597–611, doi:10.5194/angeo-30-597-2012.

Haaland, S., et al. (2015), Estimation of cold plasma outflow during geomagnetic storms, *J. Geophys. Res.*, doi:10.1002/2015JA021810, 2015JA021810.

Hamilton, D. C., G. Gloeckler, F. M. Ipavich, B. Wilken, and W. Stuedemann (1988), Ring current development during the great geomagnetic storm of February 1986, *J.*



Author Manuscript

This article is protected by copyright. All rights reserved.

*Geophys. Res.,* , *93*, 14,343–14,355, doi:10.1029/JA093iA12p14343.

Johnstone, A. D., et al. (1997), Peace: a Plasma Electron and Current Experiment, *Space Sci. Rev.*, *79*, 351–398, doi:10.1023/A:1004938001388.

Jordanova, V. K., J. U. Kozyra, A. F. Nagy, and G. V. Khazanov (1997), Kinetic model of the ring current-atmosphere interactions, *J. Geophys. Res.*, *102*(A7), 14,279–14,291, doi:10.1029/96JA03699.

Kamide, Y., and A. Chian (2007), *Handbook of the solar-terrestrial environment*, 364-367 pp., Springer, Berlin, Heidelberg, New York.

Keika, K., et al. (2016), Storm time impulsive enhancements of energetic oxygen due to adiabatic acceleration of preexisting warm oxygen in the inner magnetosphere, *J. Geophys. Res.*, *121*, 7739–7752, doi:10.1002/2016JA022384.

Kistler, L. M., E. Möbius, B. Klecker, G. Gloeckler, and F. M. Ipavich (1990), Spatial variations in the suprathermal ion distributions during substorms in the plasma sheet, *J. Geophys. Res.*, *95*, 18,871–18,885, doi:10.1029/JA095iA11p18871.

Kistler, L. M., E. Moebius, W. Baumjohann, G. Paschmann, and D. C. Hamilton (1992), Pressure changes in the plasma sheet during substorm injections, *J. Geophys. Res.*, *97*, 2973–2983, doi:10.1029/91JA02802.

Kistler, L. M., D. J. Larson, E. Möbius, and W. Baumjohann (1994), The decay of superathermal ion fluxes during the substorm recovery phase, *J. Geophys. Res.,* , *99*, 10,941–10,954, doi:10.1029/93JA03180.

Kistler, L. M., C. G. Mouikis, B. Klecker, and I. Dandouras (2010), Cusp as a source for oxygen in the plasma sheet during geomagnetic storms, *J. Geophys. Res.*, *115*, A03209, doi:10.1029/2009JA014838.



This article is protected by copyright. All rights reserved.

Kistler, L. M., C. G. Mouikis, and K. J. Genestreti (2013), In-flight calibration of the Cluster/CODIF sensor, *Geoscientific Instrumentation, Methods and Data Systems*, *2*, 225–235, doi:10.5194/gi-2-225-2013.

Krimigis, S. M., R. W. McEntire, T. A. Potemra, G. Gloeckler, F. L. Scarf, and E. G. Shelley (1985), Magnetic storm of September 4, 1984 - A synthesis of ring current spectra and energy densities measured with AMPTE/CCE, *Geophys. Res. Lett.,* , *12*, 329–332, doi:10.1029/GL012i005p00329.

Kronberg, E. A., and P. W. Daly (2013), Spectral analysis for wide energy channels, *Geoscientific Instrumentation, Methods and Data Systems Discussions*, *3*, 533–546, doi: 10.5194/gid-3-533-2013.

Kronberg, E. A., P. W. Daly, I. Dandouras, S. Haaland, and E. Georgescu (2010), Generation and Validation of Ion Energy Spectra Based on Cluster RAPID and CIS Measurements, in *The Cluster Active Archive, Studying the Earth's Space Plasma Environment*, edited by Laakso, H., Taylor, M., & Escoubet, C. P., pp. 301–306, doi: 10.1007/978-90-481-3499-1_20.

Kronberg, E. A., S. E. Haaland, P. W. Daly, E. E. Grigorenko, L. M. Kistler, M. Fränz, and I. Dandouras (2012), Oxygen and hydrogen ion abundance in the near-Earth magnetosphere: Statistical results on the response to the geomagnetic and solar wind activity conditions, *J. Geophys. Res.*, *117*, A12208, doi:10.1029/2012JA018071.

Kronberg, E. A., E. E. Grigorenko, S. E. Haaland, P. W. Daly, D. C. Delcourt, H. Luo, L. M. Kistler, and I. Dandouras (2015), Distribution of energetic oxygen and hydrogen in the near-Earth plasma sheet, *J. Geophys. Res.*, *120*, 3415–3431, doi: 10.1002/2014JA020882.



Author Manuscript

This article is protected by copyright. All rights reserved.

Kronberg, E. A., et al. (2014), Circulation of Heavy Ions and Their Dynamical Effects in the Magnetosphere: Recent Observations and Models, *Space Sci. Rev.*, *184*, 173–235, doi:10.1007/s11214-014-0104-0.

Li, K., et al. (2013), Transport of cold ions from the polar ionosphere to the plasma sheet, *J. Geophys. Res.*, *118*, 5467–5477, doi:10.1002/jgra.50518.

Liemohn, M. W., R. M. Katus, and R. Ilie (2015), Statistical analysis of storm-time near-Earth current systems, *Ann. Geophys.*, *33*, 965–982, doi:10.5194/angeo-33-965-2015.

Lyons, L. R., and D. J. Williams (1984), *Quantitative aspects of magnetospheric physics* , 8 pp., D. Reidel Publishing Company, Dordrecht, Holland.

Maggiolo, R., and L. M. Kistler (2014), Spatial variation in the plasma sheet composition: Dependence on geomagnetic and solar activity, *J. Geophys. Res.*, *119*, 2836–2857, doi: 10.1002/2013JA019517.

Moebius, E., M. Scholer, B. Klecker, D. Hovestadt, G. Gloeckler, and F. M. Ipavich (1987), *Acceleration of ions of ionospheric origin in the plasmasheet during substorm activity*, pp. 231–234, In: Magnetotail Physics, edited by A. T. Y. Lui, The Johns Hopkins University Press, Baltimore, Md.

Mouikis, C. G., L. M. Kistler, G. Wang, and Y. Liu (2014), Background subtraction for the Cluster/CODIF plasma ion mass spectrometer, *Geoscientific Instrumentation, Methods and Data Systems*, *3*, 41–48, doi:10.5194/gi-3-41-2014.

O'Brien, T. P., and R. L. McPherron (2000), An empirical phase space analysis of ring current dynamics: Solar wind control of injection and decay, *J. Geophys. Res.*, *105*, 7707–7720, doi:10.1029/1998JA000437.



This article is protected by copyright. All rights reserved.

590 Powell, K. G., P. L. Roe, T. J. Linde, T. I. Gombosi, and D. L. De Zeeuw (1999), A
591 Solution-Adaptive Upwind Scheme for Ideal Magnetohydrodynamics, *Journal of Com-*
592 *putational Physics*, *154*, 284–309, doi:10.1006/jcph.1999.6299.

593 Pulkkinen, T. I., et al. (2001), Ring current ion composition during solar minimum and
594 rising solar activity: Polar/CAMMICE/MICS results, *J. Geophys. Res.*, *106*, 19,131–
595 19,148, doi:10.1029/2000JA003036.

596 Rème, H., et al. (2001), First multispacecraft ion measurements in and near the Earth's
597 magnetosphere with the identical Cluster ion spectrometry (CIS) experiment, *Ann.*
598 *Geophys.*, *19*, 1303–1354.

599 Ridley, A. J., D. L. De Zeeuw, T. I. Gombosi, and K. G. Powell (2001), Using steady
600 state MHD results to predict the global state of the magnetosphere-ionosphere system,
601 *J. Geophys. Res.*, *106*(A12), 30,067, doi:10.1029/2000JA002233.

602 Roeder, J. L., J. F. Fennell, M. W. Chen, M. Schulz, M. Grande, and S. Livi (1996),
603 CRRES observations of the composition of the ring-current ion populations, *Advances*
604 *in Space Research*, *17*, 17–24, doi:10.1016/0273-1177(95)00689-C.

605 Schunk, R. W., and J. J. Sojka (1989), A three-dimensional time-dependent model of the
606 polar wind, *J. Geophys. Res.*, *94*(A7), 8973, doi:10.1029/JA094iA07p08973.

607 Sckopke, N. (1966), A general relation between the energy of trapped particles and
608 the disturbance field near the Earth, *J. Geophys. Res.*, *71*, 3125–3130, doi:10.1029/
609 JZ071i013p03125.

610 Sojka, J., and R. Schunk (1997), Simulations of high latitude ionospheric climatology,
611 *Journal of Atmospheric and Solar-Terrestrial Physics*, *59*(2), 207–229, doi:10.1016/
612 S1364-6826(96)00037-5.



This article is protected by copyright. All rights reserved.

Tóth, G., et al. (2005), Space Weather Modeling Framework: A new tool for the space science community, *J. Geophys. Res.*, *110*, A12226, doi:10.1029/2005JA011126.

Tóth, G., et al. (2012), Adaptive numerical algorithms in space weather modeling, *Journal of Computational Physics*, *231*, 870–903, doi:10.1016/j.jcp.2011.02.006.

Tsyganenko, N. A., and T. Mukai (2003), Tail plasma sheet models derived from Geotail particle data, *J. Geophys. Res.*, *108*, 1136, doi:10.1029/2002JA009707.

Vallat, C., et al. (2005), First current density measurements in the ring current region using simultaneous multi-spacecraft CLUSTER-FGM data, *Ann. Geophys.*, *23*, 1849–1865, doi:10.5194/angeo-23-1849-2005.

Welling, D. T., and A. J. Ridley (2010), Exploring sources of magnetospheric plasma using multispecies MHD, *J. Geophys. Res.*, *115*, A04201, doi:10.1029/2009JA014596.

Welling, D. T., V. K. Jordanova, S. G. Zaharia, A. Glocer, and G. Toth (2011), The effects of dynamic ionospheric outflow on the ring current, *J. Geophys. Res.*, *116*, A00J19, doi:10.1029/2010JA015642.

Welling, D. T., V. K. Jordanova, A. Glocer, G. Toth, M. W. Liemohn, and D. R. Weimer (2015), The two-way relationship between ionospheric outflow and the ring current, *J. Geophys. Res.*, *120*(6), 4338–4353, doi:10.1002/2015JA021231.

Welling, D. T., A. R. Barakat, J. V. Eccles, R. W. Schunk, and C. R. Chappell (2016), Coupling the Generalized Polar Wind Model to Global Magnetohydrodynamics: Initial Results, in *Magnetosphere-Ionosphere Coupling in the Solar System*, vol. 222, chap. 14, pp. 179–193, doi:10.15142/T3C88J.

Wilken, B., et al. (2001), First results from the RAPID imaging energetic particle spectrometer on board Cluster, *Ann. Geophys.*, *19*, 1355–1366.



Author Manuscript

This article is protected by copyright. All rights reserved.

Williams, D. J. (1981), Ring current composition and sources - An update, *Planet. Space Sci.*, *29*, 1195–1203, doi:10.1016/0032-0633(81)90124-0.

Yu, Y., and A. J. Ridley (2013), Exploring the influence of ionospheric o+ outflow on magnetospheric dynamics: dependence on the source location, *J. Geophys. Res.*, *118*(4), 1711–1722, doi:10.1029/2012JA018411.

Zhao, H., et al. (2015), The evolution of ring current ion energy density and energy content during geomagnetic storms based on Van Allen Probes measurements, *J. Geophys. Res.*, *120*, 7493–7511, doi:10.1002/2015JA021533.

Author Manuscript



This article is protected by copyright. All rights reserved.

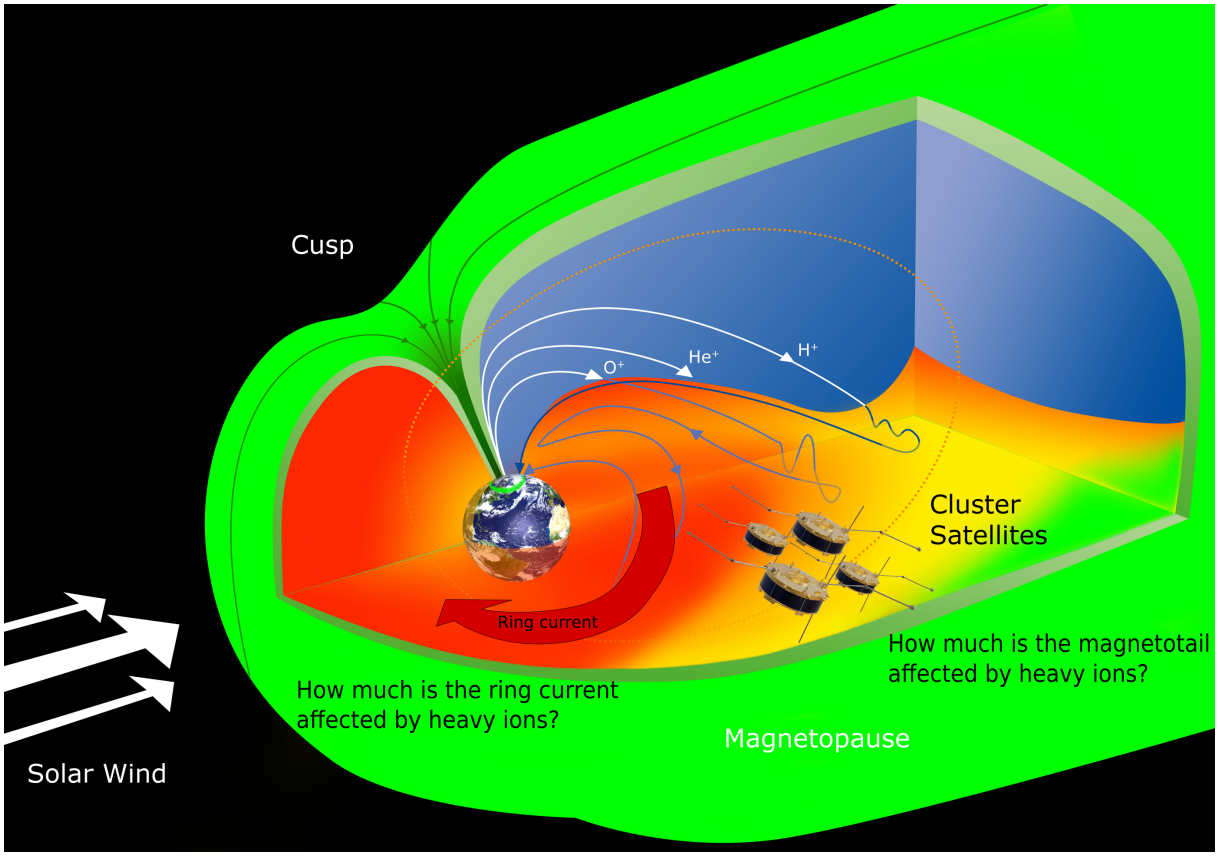



**Figure 1.** Artist's view of the circulation of ionospheric ions in the magnetosphere.

Author



This article is protected by copyright. All rights reserved.

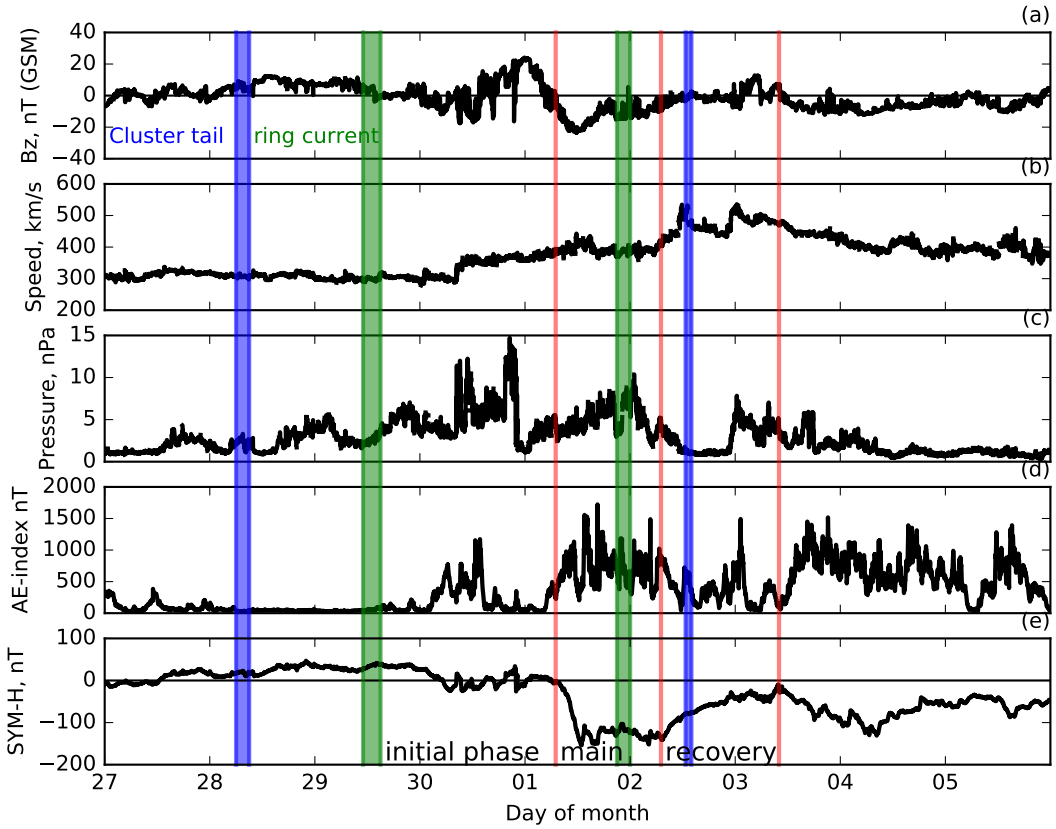



**Figure 2.** Solar wind and geomagnetic activity during the magnetic storm from Sept 27 to Oct 5, 2002 from top to the bottom: Interplanetary Magnetic Field (IMF) south-north component, $B_z$ (panel a); the solar wind speed (panel b); the solar wind dynamic pressure (panel c); the AE index (panel d) and SYM/H index (panel e). The vertical green and blue bars indicate the time periods considered further in Figures 4 and 5 for the tail (blue) and ring current regions (green). The red vertical lines outline the start of the main phase of the magnetic storm, start of the recovery phase and its end.

Author Manuscript



This article is protected by copyright. All rights reserved.

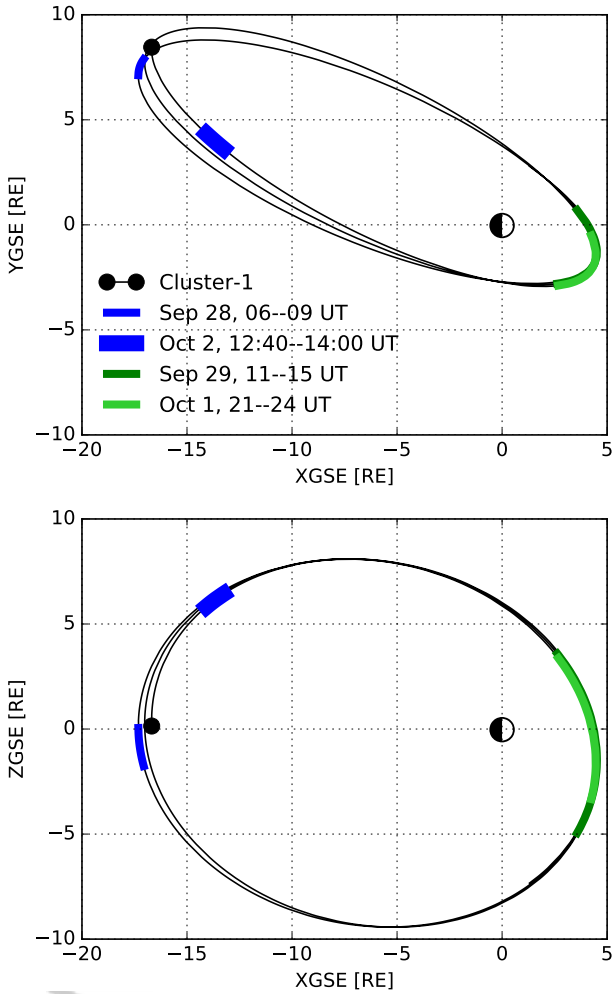



**Figure 3.** The orbit of the Cluster 1 satellite in XY and XZ GSE planes on September 29 11:00–15:00 UT.

Author M



This article is protected by copyright. All rights reserved.

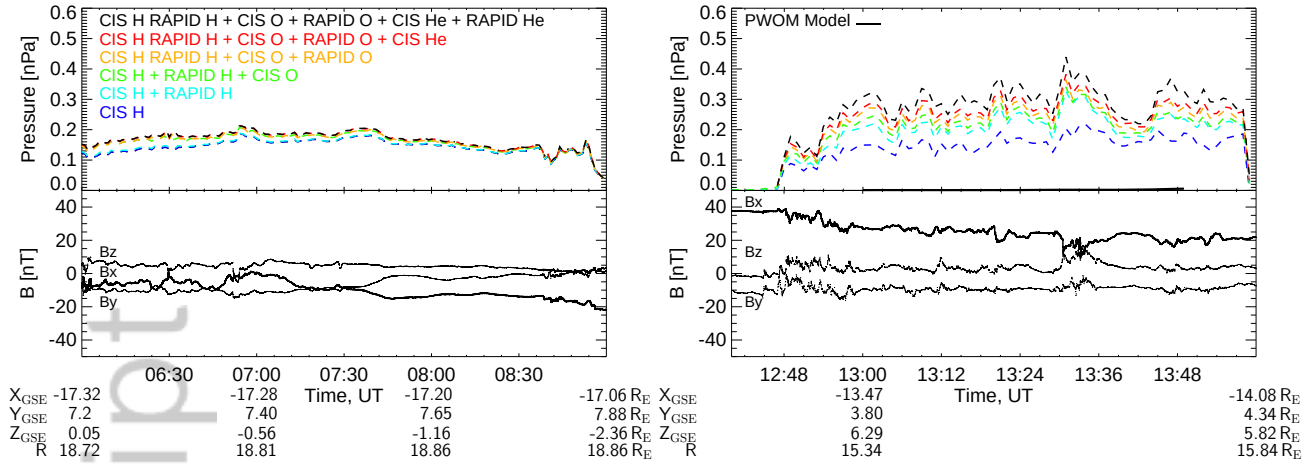



**Figure 4.** The partial pressures of protons, oxygen and helium at energy bands from 40 eV to 40 keV and >40 keV (top) and corresponding three magnetic field components in the tail region for the time period before the magnetic storm on September 28 06:00–09:00 UT (left) and during the recovery phase of the magnetic storm on October 2 from 12:40 to 14:00 (right). The meaning of the colors is: dark blue dashed line is partial pressure using only CIS $H^+$ observations, light blue is using CIS $H^+$+RAPID $H^+$, green is using CIS $H^+$+RAPID $H^+$+CIS $O^+$, yellow is using CIS $H^+$+RAPID $H^+$+CIS $O^+$+RAPID $O^+$, red is using CIS $H^+$ +RAPID $H^+$+CIS $O^+$+RAPID $O^+$+CIS $He^+$, black is using CIS $H^+$+ RAPID $H^+$+CIS $O^+$+ RAPID $O^+$+ CIS $He^+$ +RAPID $He^+$. The black solid line (upper-right panel) indicates the plasma pressure derived from the SWMF/PWOM model for the recovery phase of the magnetic storm. The pressure is not zero but has low values because virtual Cluster is still in the lobe. The magnetospheric geometry is not good enough for this part of the simulation. Therefore, the SWMF is missing the plasma sheet encounter.

Author Manuscript



This article is protected by copyright. All rights reserved.

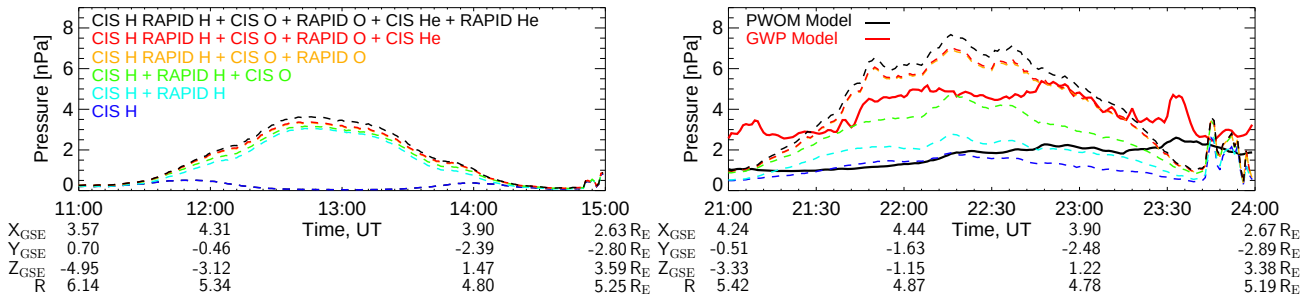



**Figure 5.** The partial pressures of protons, oxygen and helium at energy bands from 40 eV to 40 keV and >40 keV in the ring current region for the time period before the magnetic storm on September 29 11:00–15:00 UT (left) and during the main phase of the magnetic storm on October 1 from 21:00 to 24:00 (right). The black and red solid lines indicate the plasma pressure derived from the SWMF/PWOM and SWMF/GPW models for the main phase of the magnetic storm.

**Table 1.** The contribution of the different ion species at different energies to the total pressure in %.

| $P_{H^+CIS}$ | $P_{H^+RAPID}$ | $P_{O^+CIS}$ | $P_{O^+RAPID}$ | $P_{He^+CIS}$ | $P_{He^+RAPID}$ |
|---|---|---|---|---|---|
| September 28, 2002 07:00 – 07:30 UT: before storm, tail | | | | | |
| 86.1% | 1.2% | 8.9% | 0.03% | 3.5% | 0.27% |
| September 29, 2002 22:00 – 22:30 UT: before storm, ring current | | | | | |
| 1.4% | 82.9% | 3.1% | 4.6% | 0.9% | 7.1% |
| October 1, 2002 12:40 – 13:00 UT: main phase, ring current | | | | | |
| 23.8% | 11.3% | 26% | 29.5% | 1.3% | 8.1% |
| October 2, 2002 13:00 – 13:40 UT: recovery phase, tail | | | | | |
| 51.2% | 21.2% | 5.4% | 6.7% | 4.7% | 10.8% |

Author Manuscript



This article is protected by copyright. All rights reserved.

**Table 2.** Ratio of the partial plasma pressures before and during the storm.

| $P_{H^+CIS}$ | $P_{H^+RAPID}$ | $P_{O^+CIS}$ | $P_{O^+RAPID}$ | $P_{He^+CIS}$ | $P_{He^+RAPID}$ |
|---|---|---|---|---|---|
| Ratio for the tail plasma sheet during/before | | | | | |
| 0.96 | 28.4 | 0.99 | 357 | 2.19 | 65.7 |
| Ratio for the ring current during/before | | | | | |
| 33.96 | 0.27 | 17.06 | 2.09 | 2.7 | 2.28 |

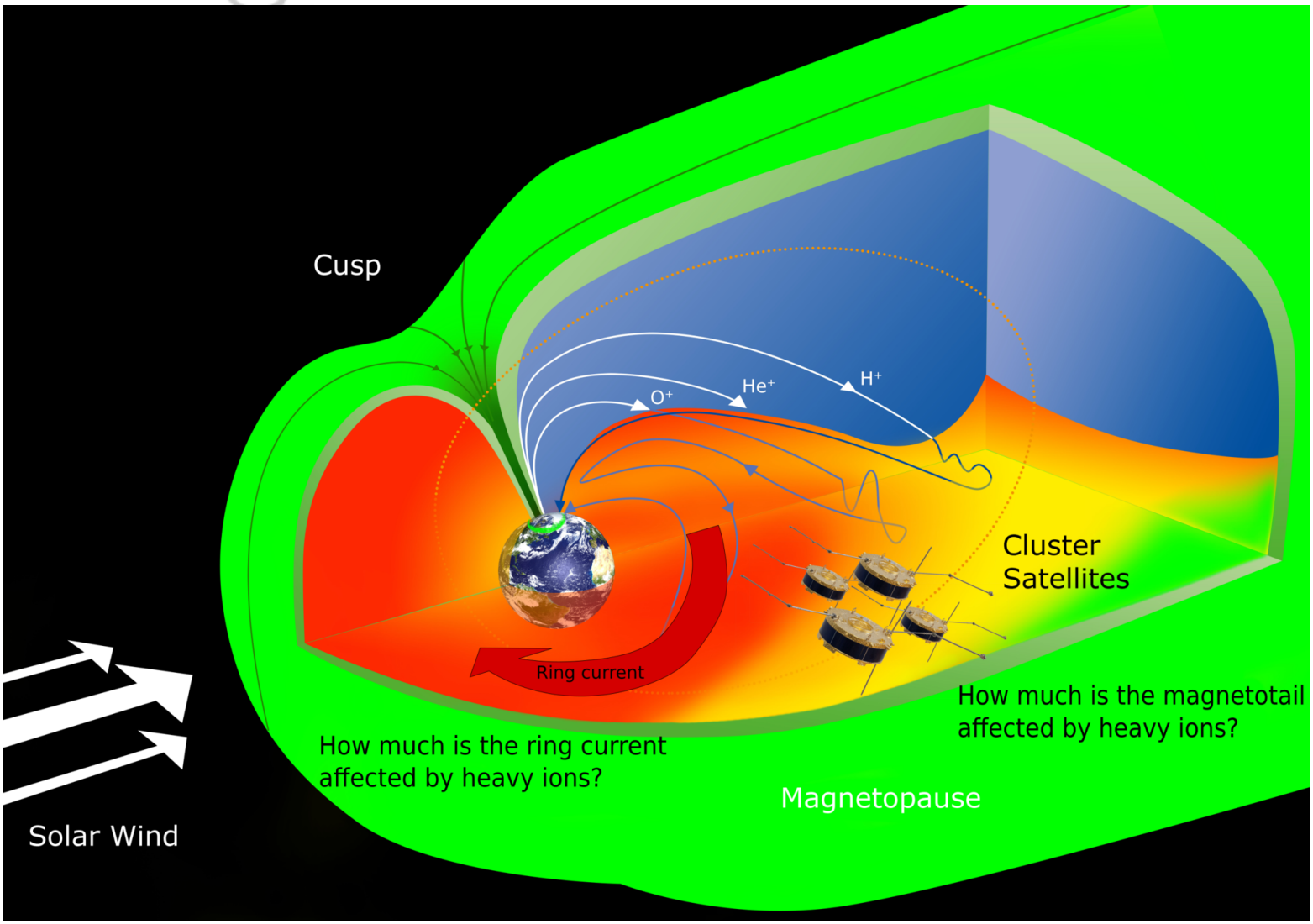
**Table 3.** Ratio of the low-energy to energetic pressures of different species before and during the storm.

| | $H^+$ | $O^+$ | He |
|---|---|---|---|
| tail plasma sheet | | | |
| Before $P_{CIS}/P_{RAPID}$ | 71 | 295 | 13.1 |
| During $P_{CIS}/P_{RAPID}$ | 2.4 | 0.82 | 0.44 |
| ring current | | | |
| Before $P_{CIS}/P_{RAPID}$ | 0.02 | 0.67 | 0.13 |
| During $P_{CIS}/P_{RAPID}$ | 2.1 | 0.87 | 0.16 |

Author Manuscript

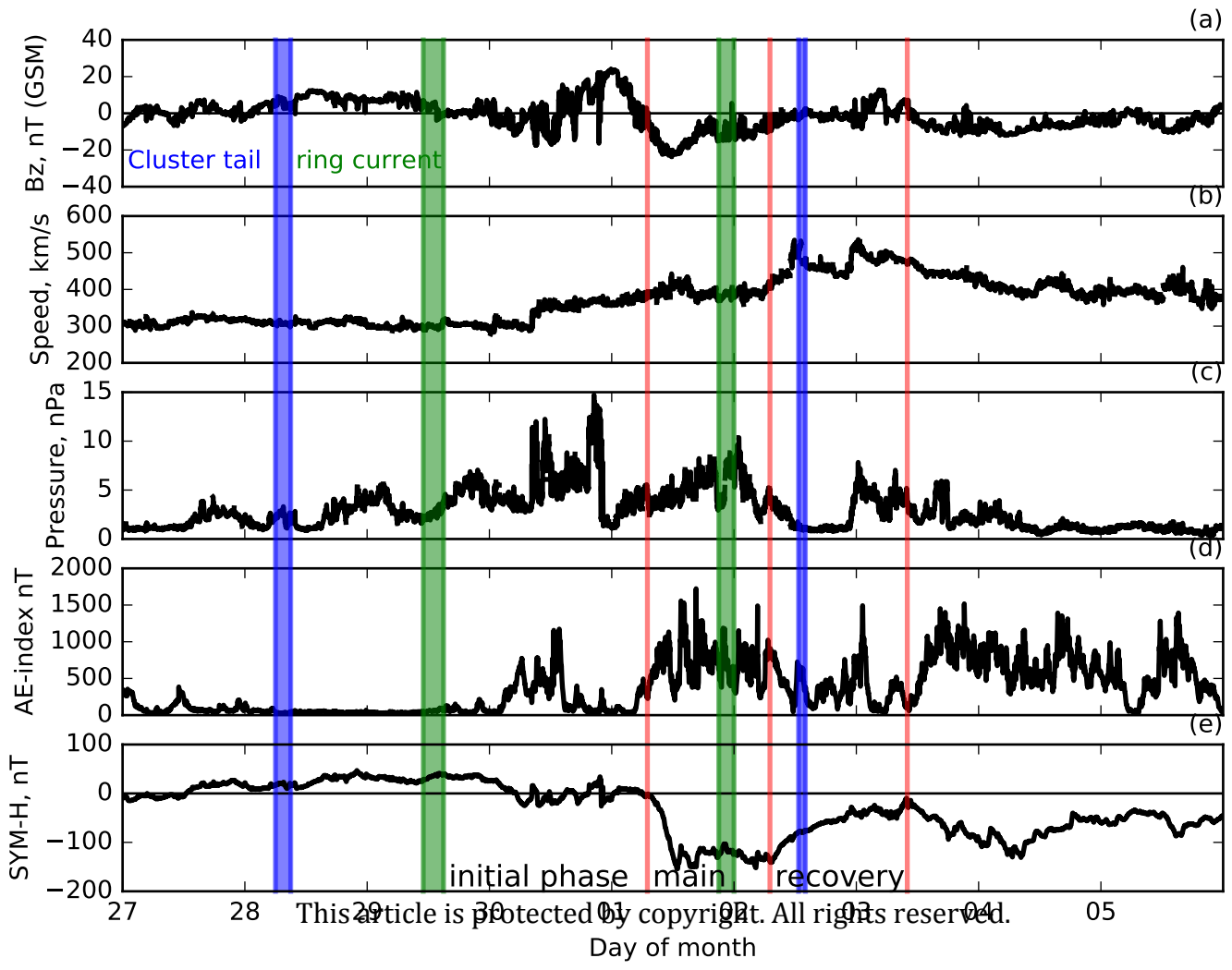


This article is protected by copyright. All rights reserved.

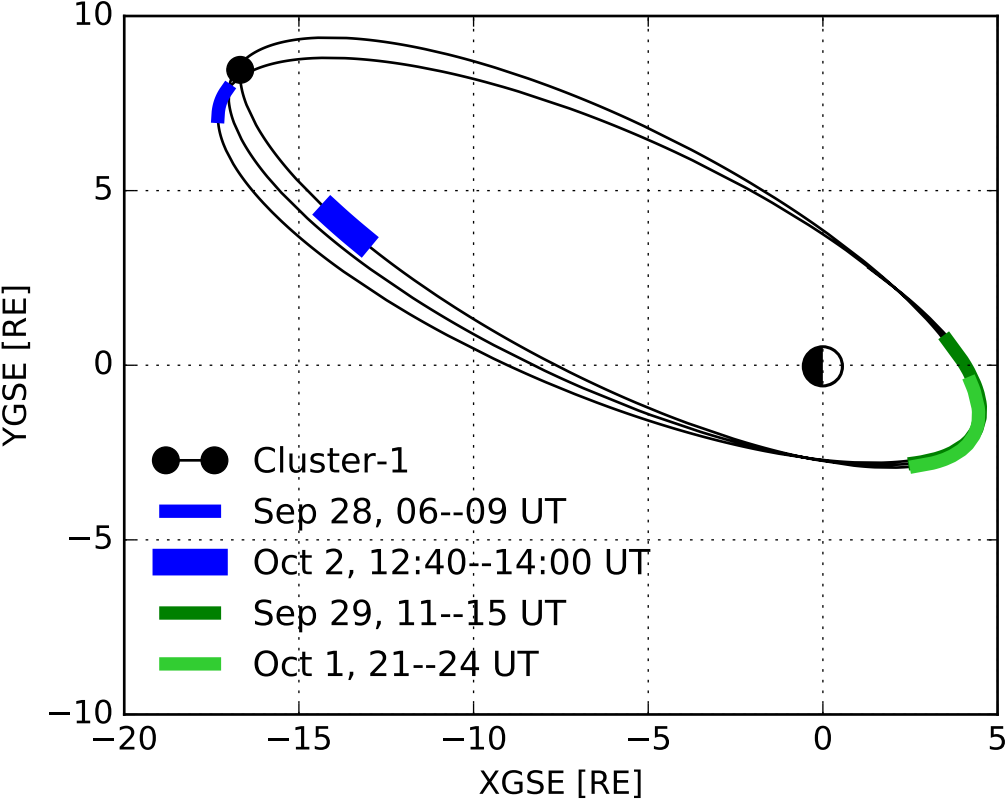


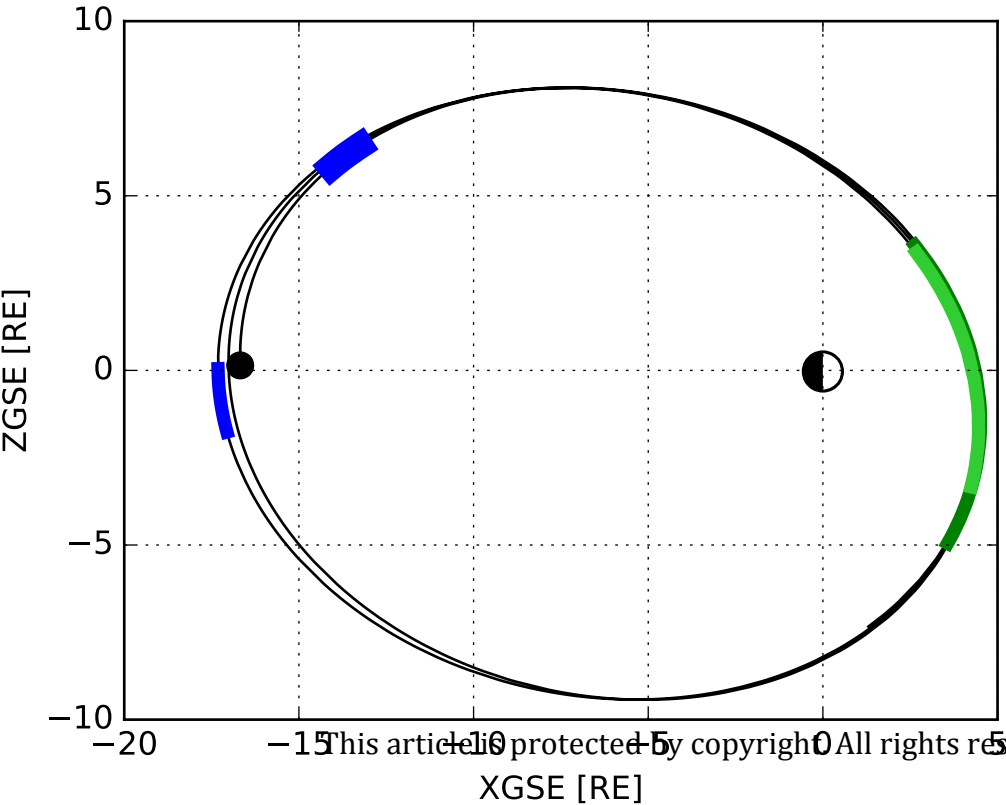

2017JA024215-f01-z-_AA.png

This article is protected by copyright. All rights reserved.

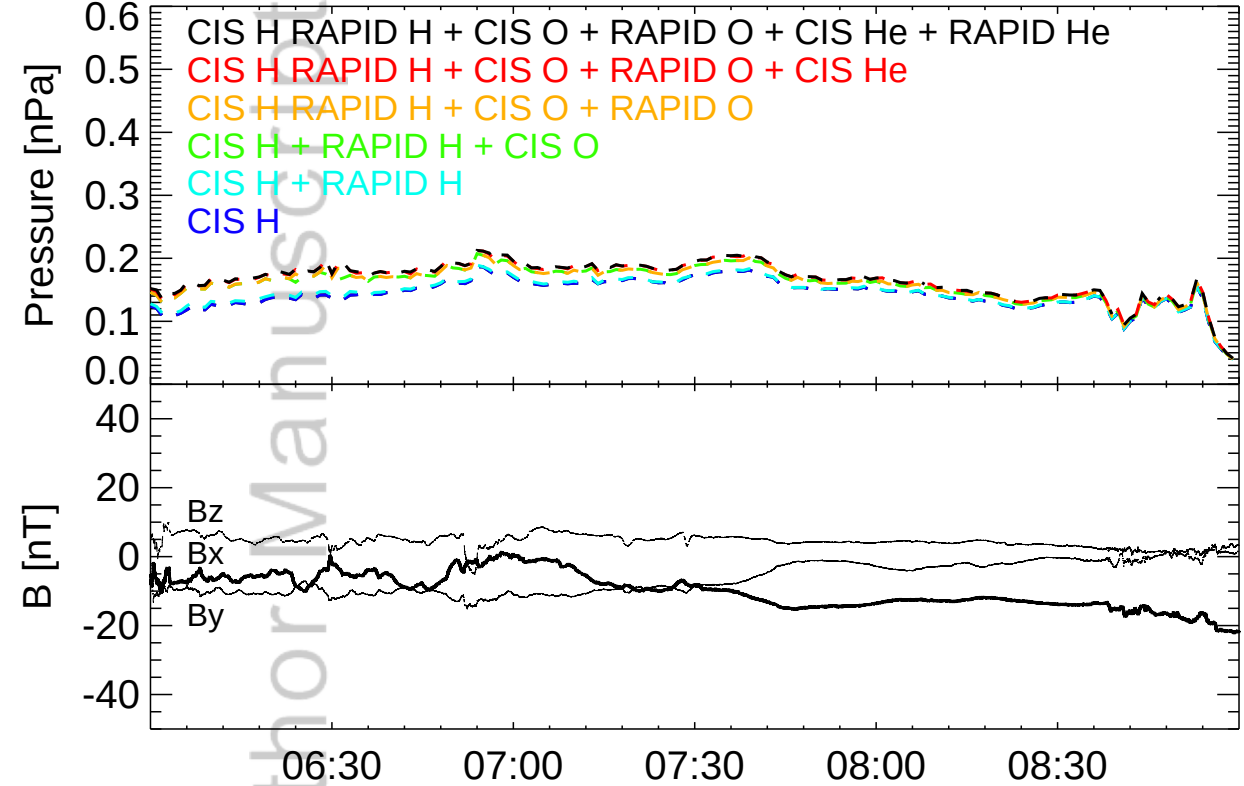



This article is protected by copyright. All rights reserved.



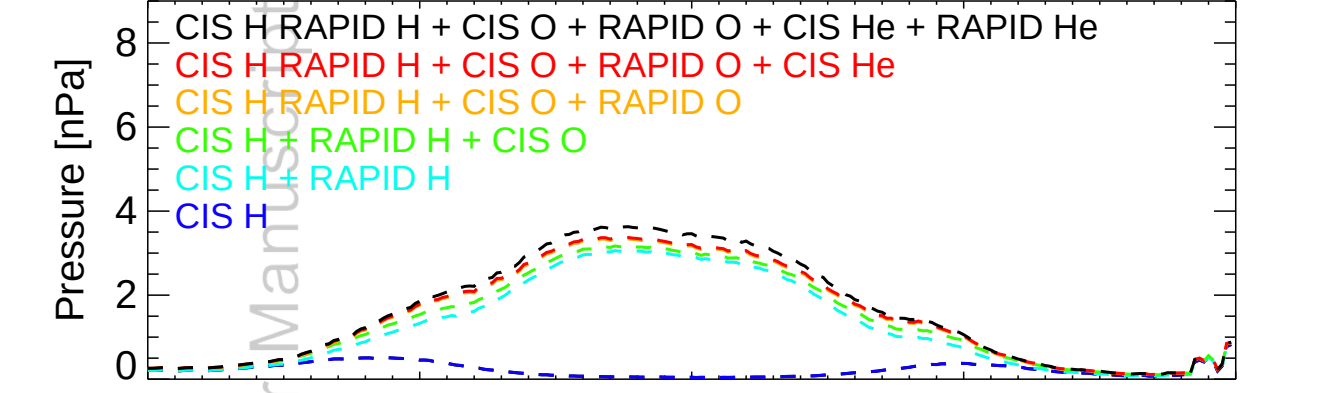

This article is protected by copyright. All rights res




| | | | | |
|---|---|---|---|---|
| $X_{GSE}$ | -17.32 | -17.28 | -17.20 | -17.06 $R_E$ |
| $Y_{GSE}$ | 7.2 | 7.40 | 7.65 | 7.88 $R_E$ |
| $Z_{GSE}$ | 0.05 | -0.56 | -1.18 | -2.36 $R_E$ |
| R | 18.72 | 18.81 | 18.86 | 18.86 $R_E$ |

This article is protected by copyright. All rights reserved.

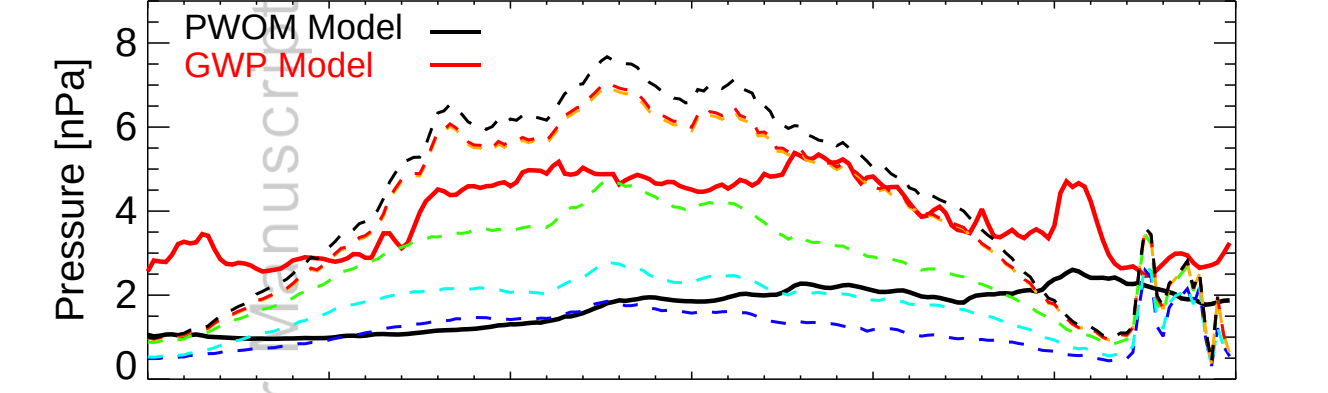
Author Manuscript




| | | | | | |
|---|---|---|---|---|---|
| $X_{GSE}$ | 3.57 | 4.31 | | 3.90 | 2.63 $R_E$ |
| $Y_{GSE}$ | 0.70 | -0.46 | | -2.39 | -2.80 $R_E$ |
| $Z_{GSE}$ | -4.95 | -3.12 | | 1.47 | 3.59 $R_E$ |
| R | 6.14 | 5.34 | | 4.80 | 5.25 $R_E$ |

Author Manuscript

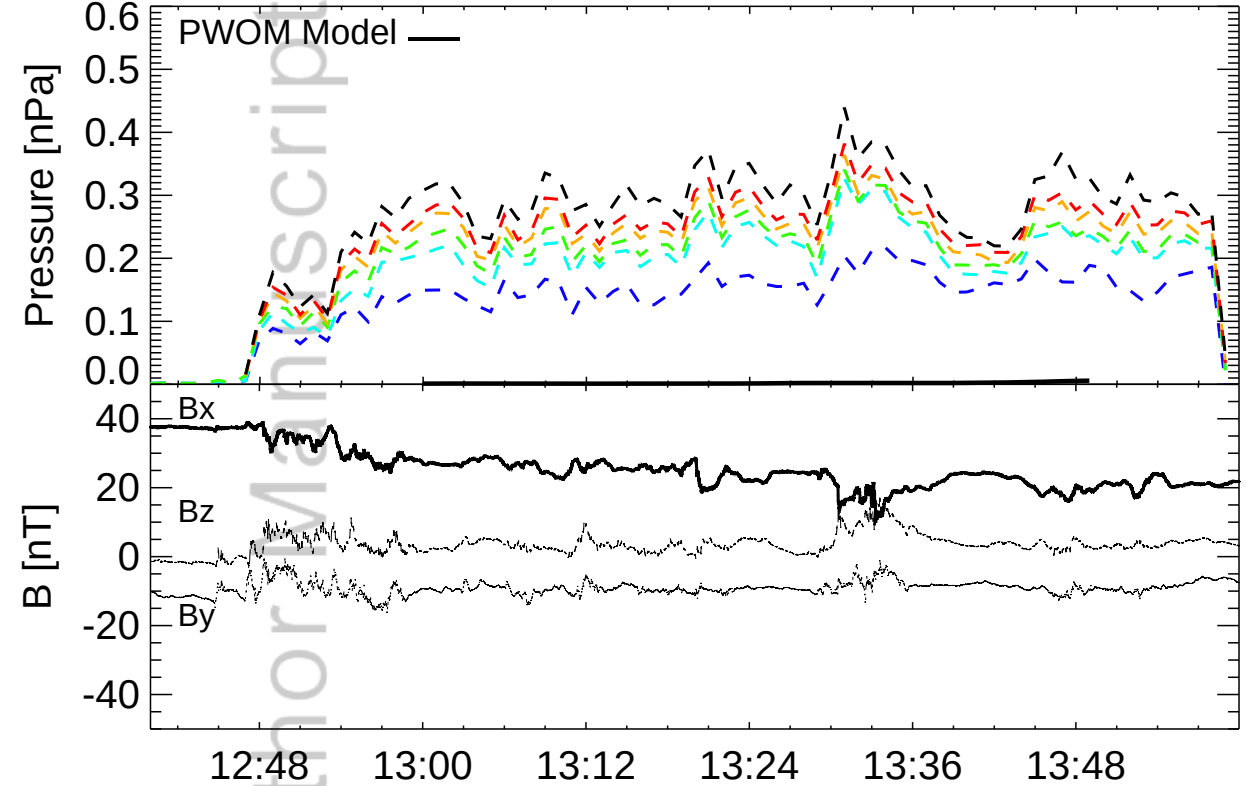
This article is protected by copyright. All rights reserved.




| | | | | |
|---|---|---|---|---|
| $X_{GSE}$ | 4.24 | 4.44 | 3.90 | 2.67 $R_E$ |
| $Y_{GSE}$ | -0.51 | -1.63 | -2.48 | -2.89 $R_E$ |
| $Z_{GSE}$ | -3.33 | -1.15 | -1.22 | 3.38 $R_E$ |
| R | 5.42 | 4.87 | 4.78 | 5.19 $R_E$ |

Author Manuscript

This article is protected by copyright. All rights reserved.




| | | | |
|---|---|---|---|
| $X_{GSE}$ | -13.47 | | -14.08 $R_E$ |
| $Y_{GSE}$ | 3.80 | | 4.34 $R_E$ |
| $Z_{GSE}$ | 6.29 | | 5.82 $R_E$ |
| R | 15.34 | | 15.84 $R_E$ |

This article is protected by copyright. All rights reserved.

Author Manuscript